Noise prediction of Vertical Axis Wind Turbines

21000269 | Linus Adzanku

Module: UFMEWD-15-M - Aero-acoustics

Literature Review

Current State of VAWT Research

- Renewed interest in VAWTs for climate and urban energy; HAWTs still dominate (>90% market) due to higher efficiency (Lee, 2024)
- VAWTs suffer larger wake losses, dynamic stall and vortex-induced turbulence, so typical Cp (power coefficient) is lower than HAWTs (Lee, 2024)
- VAWTs are omni-directional (no yaw), easier low-wind operation, lower manufacturing/maintenance costs (no yaw gear) and smaller footprint (Lee, 2024)
- Well-suited to complex flows (urban rooftops, offshore, wake-heavy sites) and can be sited near storage to cut transmission losses (Lee, 2024)

Current State of VAWT Research – cont'd

- Two main types – *lift-driven* Darrieus rotors (slender aerofoil blades) and *drag-driven* Savonius rotors (curved vanes). Savonius turbines are self-starting but low-efficiency (~Cp≈0.15–0.20) (Abdolahifar, 2024). Darrieus rotors have higher peak Cp (~0.30–0.40 for bare 3-blade VAWTs) but require external start assistance (Chen, 2024).
- Geometric optimizations (pitch angle, chord/radius, solidity) and additions (shrouds, diffusers) are actively studied. For example, adding optimized deflectors has raised Cp from ~0.37 (bare) to ~0.63 (70% increase) at $\lambda \approx 2.3$.
- Adaptive flaps and leading-edge modifications can boost lift and efficiency.
- Many recent studies focus on variable-pitch, adaptive blades, and hybrid designs (e.g. Darrieus - Savonius) to improve starting and widen operational range. However, complexity and cost of such mechanisms remain as challenges. (Lee, 2024)

The Darreius VAWT

- Darrieus VAWTs use rotating aerofoils to generate lift perpendicular to axis (Lee,2024) . They produce power over a range of λ (typically 2–6) and can achieve ~30–40% peak Cp in practice.
- Blades experience cyclic angle-of-attack:
  - Leading half sees high relative wind
  - Trailing half sees wake.
  - This causes dynamic stall, strong negative torque spikes and vortex shedding each revolution.
- Blade vortex shedding and laminar-turbulent boundary-layer transitions produce aerodynamic noise. In model tests, blade self-noise (from laminar instabilities) dominated, while pure blade-passing tones were weak (Pearson, no date)

The Darreius VAWT – cont’d

- Darrieus VAWTs have lower absolute power output than similarly sized HAWTs because of 2D flow losses and cyclic stall. They spin slower, reducing broadband noise compared to fast HAWT tips (Abdolahifar, 2024).
- Adaptive flaps (trailing-edge or leading-edge) and Gurney flaps have shown large lift boosts and even noise reductions (Lee, 2024).
- Typical 3-blade Darrieus often runs at tip-speed ratios $\lambda \approx 3–5$ for max power (Chen, 2024).

State of VAWT Acoustic Research

- Noise for small/urban VAWTs is a critical issue, but systematic aeroacoustics studies are recent. Early VAWT research (1970s–’90s) focused on aerodynamics; acoustic research only picked up in 2000s with CFD and limited experiments (Pearson, no date).
- Graham & Pearson found in wind-tunnel tests that blade self-noise (from laminar separation bubbles and trailing-edge turbulence) dominates.
  - At off-design speeds, blade-passage tones were minor.
  - Increasing tip-speed ratio strongly raises noise
- VAWT noise has tonal and broadband components. Findings show that these components are unimportant (Pearson, no date).
- CFD/LES studies report ~ 40 dB(A) (75 dB non A-weighted) at the 3-blade passing tone (40 Hz). In contrast, high-frequency laminar-turbulence tones (>1 kHz) can reach ~60 dB, which is significant for human annoyance as A-weighting does no attenuate the amplitude (Viqueira, 2020).

State of VAWT Acoustic Research – cont'd

- Most recent VAWT noise studies use CFD+acoustics.
- In many papers, LES has been used to compute aeroacoustic spectra of isolated and farmed VAWTs. These simulations identify blade-wake interactions and boundary-layer turbulence as primary sound sources (Viqueira, 2020)..
- In turbine clusters, noises do not superimpose one another linearly. Interactions and wake scattering alter directivity and reduce some mid-frequency tones. Farms however, do not eliminate the main tonal frequencies (blade passing, separation tones) seen on isolated rotors (Viqueira, 2020).
- Recommended ambient noise limits (e.g. ~40 dB(A) in residential zones) imply VAWTs must be quiet. Few papers target specific dB goals, but measured A-weighted levels suggest small VAWTs can meet standards if well-designed (i.e.. slow rotors, noise-optimized blades).
- Reducing tip speed and aerofoil trailing-edge roughness can mitigate noise generation.

Numerical Methods

- Unsteady RANS (URANS) is common (e.g. SST k–ω or realizable k–ε models) for VAWT flow field simulation due to lower cost. Higher-fidelity LES or DES are increasingly used to capture tonal noise and flow instabilities (Viqueira, 2020).
- Accurate aeroacoustics require fine meshes. Wall-resolved grids ($y^+ \approx 1$) are needed to capture boundary layers and laminar-turbulent transition. Viqueira (2020) conducted a study using a WALE-LES model, where only the fine mesh case captured the expected tonal peak from a NACA0012 profile
- Typical grids span millions of cells around the rotor. Moving mesh or sliding-domain techniques handle blade rotation. Time-stepping must be small enough to resolve blade passage (e.g. >200 steps per revolution). Subsonic low-Mach assumption holds, but care is taken to resolve small turbulent scales that generate noise.

Numerical Methods – cont'd

- The Ffowcs–Williams Hawkings (FW–H) analogy is the standard tool. CFD provides unsteady surface pressures and velocities on blades, and FW–H (surface or permeable form) computes far-field noise (dipole/quadrupole sources) (Pearson, no date).
- Commercial codes (e.g. ANSYS Fluent) integrate URANS flow solvers with FW–H acoustic modules; some also offer CAA (wave-equation) solvers. For instance, Wang et al. (2024) coupled Fluent URANS with FW–H to study a 5 kW VAWT's noise
- In aeroacoustic analogy, blade surface pressure fluctuations (dipoles) dominate VAWT noise; free-stream turbulence noise is comparatively small. Thus, modelling focuses on blade surface sources (including serrations or flaps).
- Simulations are validated against experimental spectra or trusted cases (e.g. NACA0012 in flow). The known tonal behaviour of simple aerofoils is used to check acoustic output (e.g. matching main tone and harmonics) (Viqueira et. al, 2020).

Current Gaps and Future directions

- There is a lack of full-scale experimental acoustic data for VAWTs, especially in real wind/farm conditions. Most literature covers small models or 2D simulations; *in-situ* measurements would validate and tune models.
- Further 3D-LES/DES studies are needed to capture complex VAWT flow (blade-vortex interactions, dynamic stall) and fully predict noise. Coupled aeroelastic (FSI) models could also reveal vibration/noise coupling.
- More research on acoustic interaction in turbine arrays and built environments is needed. For instance, how do multiple VAWTs on rooftops combine noise? Can shielding (e.g. trees, berms) or smart placement minimize community impact? (Wang et. al, 2024)

Summary

- While VAWTs offer advantages (omni-directionality, low-speed operation, simplicity), their aerodynamics and aeroacoustics remain complex.
- The reviewed literature highlights key performance trade-offs and noise sources, but addressing these in a holistic way (performance, noise, cost) is an ongoing challenge.
- Continued high-fidelity studies and experiments will push VAWTs towards practical urban and renewable-energy applications.

References

- Abdolahifar, A. and Zanj, A. (2024) Addressing VAWT Aerodynamic Challenges as the Key to Unlocking Their Potential in the Wind Energy Sector. Energies [online]. 17 (20), p. 5052. Available from: https://www.mdpi.com/1996-1073/17/20/5052 [Accessed 9 December 2024].
- Chen, W.-H., Lam, T.T., Chang, M.-H., Jin, L., Chih-Che Chueh and Augusto, G.L. (2024) Optimizing H-Darrieus Wind Turbine Performance with Double-Deflector Design. Energies [online]. 17 (2), pp. 503–503. [Accessed 9 December 2024].
- Lee, K.-Y., Cruden, A., Ng, J.-H. and Wong, K.-H. (2024) Variable designs of vertical axis wind turbines—a review. Frontiers in Energy Research [online]. 12. [Accessed 5 December 2024].
- Pearson, C.E. and Graham, W.R. (no date) Noise from a Model-Scale Vertical-Axis Wind Turbine [online]. Available from: https://api.repository.cam.ac.uk/server/api/core/bitstreams/9be62e42-5c4e-4ffe-9666-f853635bfa69/content [Accessed 8 December 2024].
- Viqueira-Moreira, M. and Ferrer, E. (2020) Insights into the Aeroacoustic Noise Generation for Vertical Axis Turbines in Close Proximity. Energies [online]. 13 (16), p. 4148. [Accessed 15 December 2024].
- Wang, W.-Y. and Yuh-Ming Ferng (2024) Numerical model for noise reduction of small vertical-axis wind turbines. Wind energy science (Print) [online]. 9 (3), pp. 651–664. [Accessed 15 December 2024].

Case Study

Abstract and Problem Introduction

- Vertical axis wind turbines (VAWTs) are a promising urban energy solution, but their acoustic characteristics remain understudied, remaining a challenge for urban certification
- This study investigates a 3-blade Darrieus VAWT operating at a high tip-speed ratio (TSR = 3.3), where dynamic stall, control instability, and turbulence-induced drag degrade performance (Ma et al, 2019).
- The simulation aims to replicate aerodynamic performance from Syawitri et al. (2020), and applies the FW-H analogy to predict far-field acoustic output.
- The use of a relatively large timestep ($\Delta t = 3\times10^{-4}$ s) limits the acoustic resolution to low frequencies, which restricts full characterisation of the human-audible range.

Reference Paper

- Syawitri, T.P., Yao, Y., Yao, J., Chandra, B. - Assessment of stress-blended eddy simulation model for accurate performance prediction of vertical axis wind turbine
  - Use of Transition SST + SBES using Ansys Fluent
  - Turbulence model chosen to resolve trailing tip vortices and study effects at a range of TSRs

A summary of the differences between the reference paper and this study:

Parameter	Syawitri et al. (2020)	This Study
Turbulence Model	Transition SST + SBES	Transition SST + SBES
TSR	Range(1.44 – 3.3) 3.09 used for convergence study	3.3
BOI Resolution	Division based	Inflation layer + Element size
Timestep	$1^\circ \approx 3x10^{-4}s$	$1^\circ \approx 3x10^{-4}s$

The TSST+SBES Model

- The Transition SST + SBES model is a hybrid approach combining near-wall RANS (via SST) with LES-like resolution in separated regions.
- It is particularly well-suited for capturing vortex shedding and dynamic stall phenomena in rotating flows like VAWTs, with lower computational cost than full LES (ANSYS 2024 R2 Fluent Theory Guide, 2025).
- At its core are the governing equations for the LES model seen below (ANSYS CFX-Solver Theory Guide, 2021).

$$\frac{\partial}{\partial t}(\bar{\rho}\bar{U}_i)+\frac{\partial}{\partial x_j}(\bar{\rho}\bar{U}_i\bar{U}_j)=-\frac{\partial \bar{p}}{\partial x_i}+\frac{\partial}{\partial x_j}[\mu(\frac{\partial \bar{U}_i}{\partial x_j}+\frac{\partial \bar{U}_j}{\partial x_i})]+\frac{\partial \tau_{ij}}{\partial x_j}$$ → Filtered Navier-Stokes momentum equation

$$\tau_{ij}=-\overline{\rho U_i U_j}+\bar{\rho}\bar{U}_i\bar{U}_j$$ → Sub-grid scale stress

Governing Equations

The TSST + SBES model governs all simulations performed as part of this study.

- The Transition SST model is governed by the following in Fluent:

$$\frac{\partial}{\partial t}(\rho k) + \frac{\partial}{\partial x_j}(\rho u_j k) = \widetilde{P_k} - \widetilde{D_k} + \frac{\partial}{\partial x_j}\left((\mu + \sigma_k \mu_t)\frac{\partial k}{\partial x_j}\right)$$

$$R_y = \frac{\rho y \sqrt{k}}{\mu}$$

$$F_3 = e^{-}\left(\frac{R_y}{120}\right)^3$$

$$\widetilde{P_k} = \gamma_{eff} P_k$$

$$\widetilde{D_k} = min(max(\gamma_{eff}, 0.1), 1.0) D_k$$

$$F_t = max(F_{1orig}, F_3)$$

Because SBES switches between RANS (transition sst) and LES, when resolving LES zones, the filtered Navier stokes equations and subgrid-scale tensor are used

- The SBES model is governed by the following equations:

$$\tau_{ij}^{\mathrm{SBES}} = f_{\mathrm{SDES}} \tau_{ij}^{\mathrm{RANS}} + \left(1 - f_{\mathrm{SDES}}\right) \tau_{ij}^{\mathrm{LES}}$$

$$\nu_t^{\mathrm{SBES}} = f_{\mathrm{SDES}} \nu_t^{\mathrm{RANS}} + \left(1 - f_{\mathrm{SDES}}\right) \nu_t^{\mathrm{LES}}$$

Filtered Navier Stokes

$$\frac{\partial}{\partial t}(\rho \bar{u}_i) + \frac{\partial}{\partial x_j}(\rho \bar{u}_i \bar{u}_j) = \frac{\partial}{\partial x_j}(\sigma_{ij}) - \frac{\partial \bar{p}}{\partial x_i} - \frac{\partial \tau_{ij}}{\partial x_j}$$

Subgrid-scale

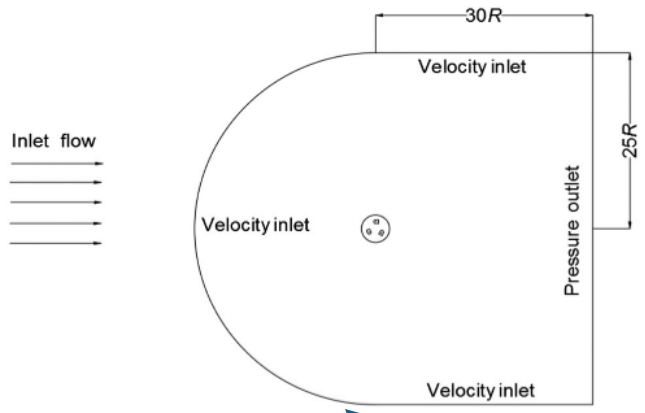
$$\tau_{ij} \equiv \rho \overline{u_i u_j} - \rho \bar{u}_i \bar{u}_j$$

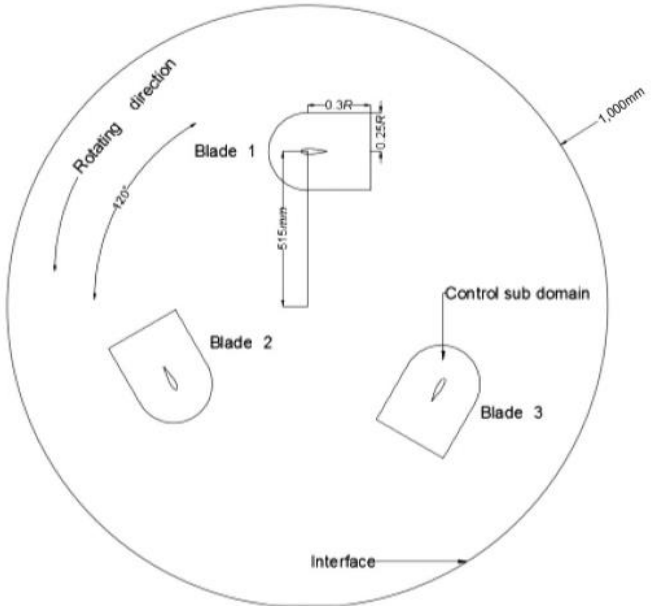
Equations from Ansys Fluent 2024 R2 & 12.0 Theory Guides

Methodology and Simulation Strategy

- This study uses the standard 3-bladed Darrieus VAWT geometry from Castelli (2011), with numerical methods and validation procedures aligned with Syawitri et al. (2020).
  - Geometry and Mesh: Castelli rotor shape implemented in 2D, with mesh refinement near the blades (BOI) and $y^+ \approx 1$ inflation layers
  - Solver: Transition SST + SBES
  - Validation: Cp, Cl, Cd and moment compared to experimental and CFD references
  - FW-H analogy used to compute acoustics; 4 omni-directional receivers placed 1 m from rotor centre
- Flow Characteristics:

Density (kg/m^3)	1.225
Temperature (K)	293.15
Pressure (Pa)	101325
Freestream Velocity (m/s)	9
Reynolds number	172,465
Dynamic Viscosity (Pa.s^{-1})	1.81x10^{-5}
Tip speed ratio	3.3





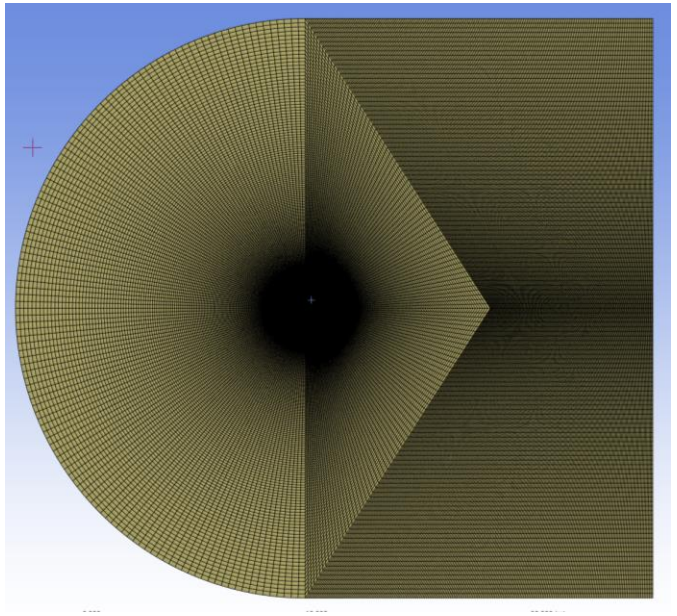
Geometry Setup. Source: Syawitri et al. 2020

Mesh Structure & CFD Setup

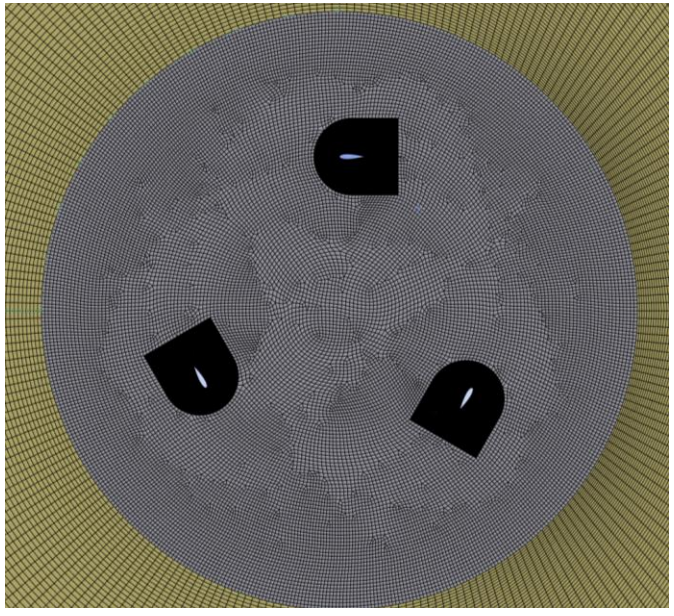
- Element sizes:
  - Body of Influence = 3.5mm
  - Rotating Core = 12mm
  - Farfield = 50mm
- Number of aerofoil divisions:
  - Upper/Lower Surface = 174
  - Blunted Trailing Edge = 14

- Uses sliding mesh technique
  - Aerofoils are placed in rotating domain – rotated about the origin
- Refined BOI around aerofoils are used to resolve trailing tip vortices
- Aerofoils, rotating domain and bodies of influence(BOIs) are surrounded by static far-field
- All domain sizes and meshing strategies are according to reference paper

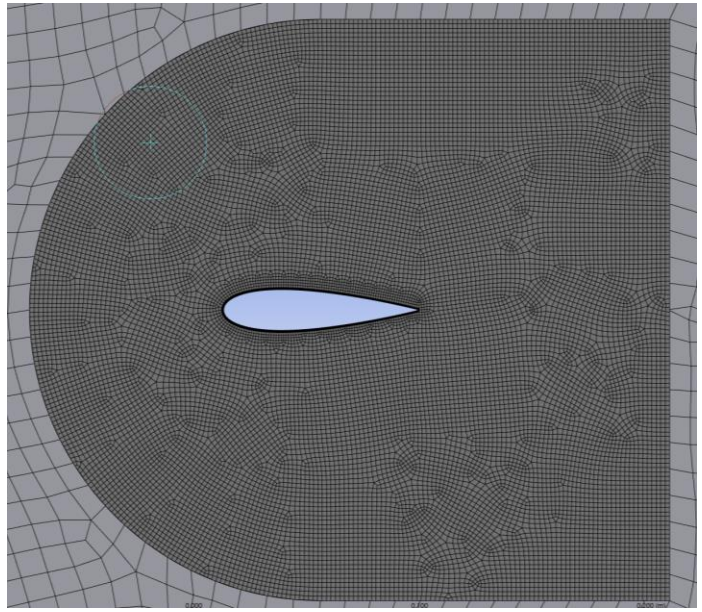
Far-field



Rotating Core



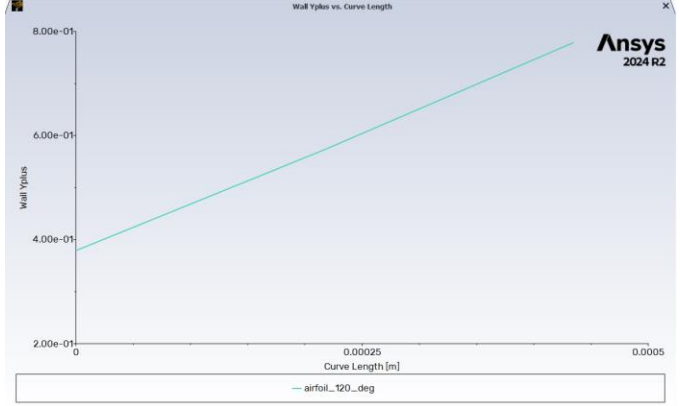
Body-of-Influence (BOI)

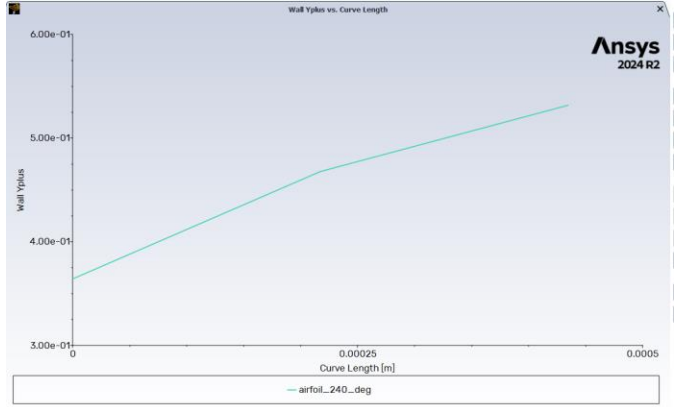


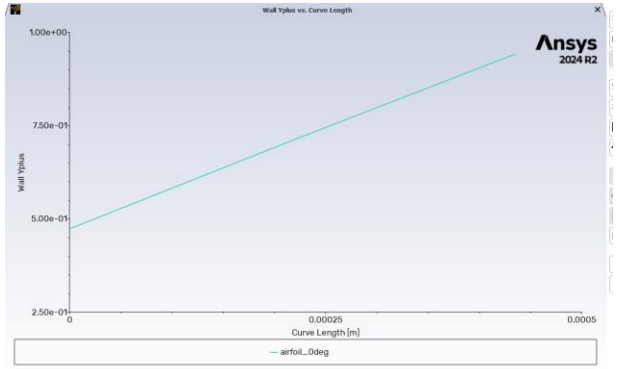
Near Wall (y+) Analysis

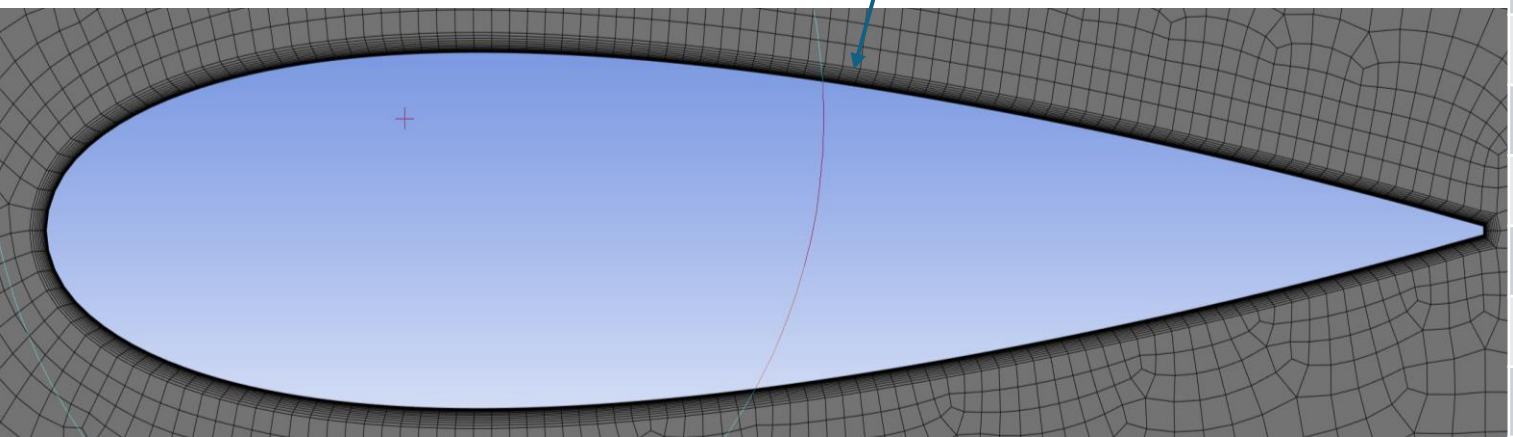
- y+ ~= 1 maintained around all aerofoils
- No slip condition
- Boundary layer was modelled using inflation layers calculated using an online calculator (FluidMechanics101.com, no date).

$$y^+ = \frac{u_* y}{\nu}$$







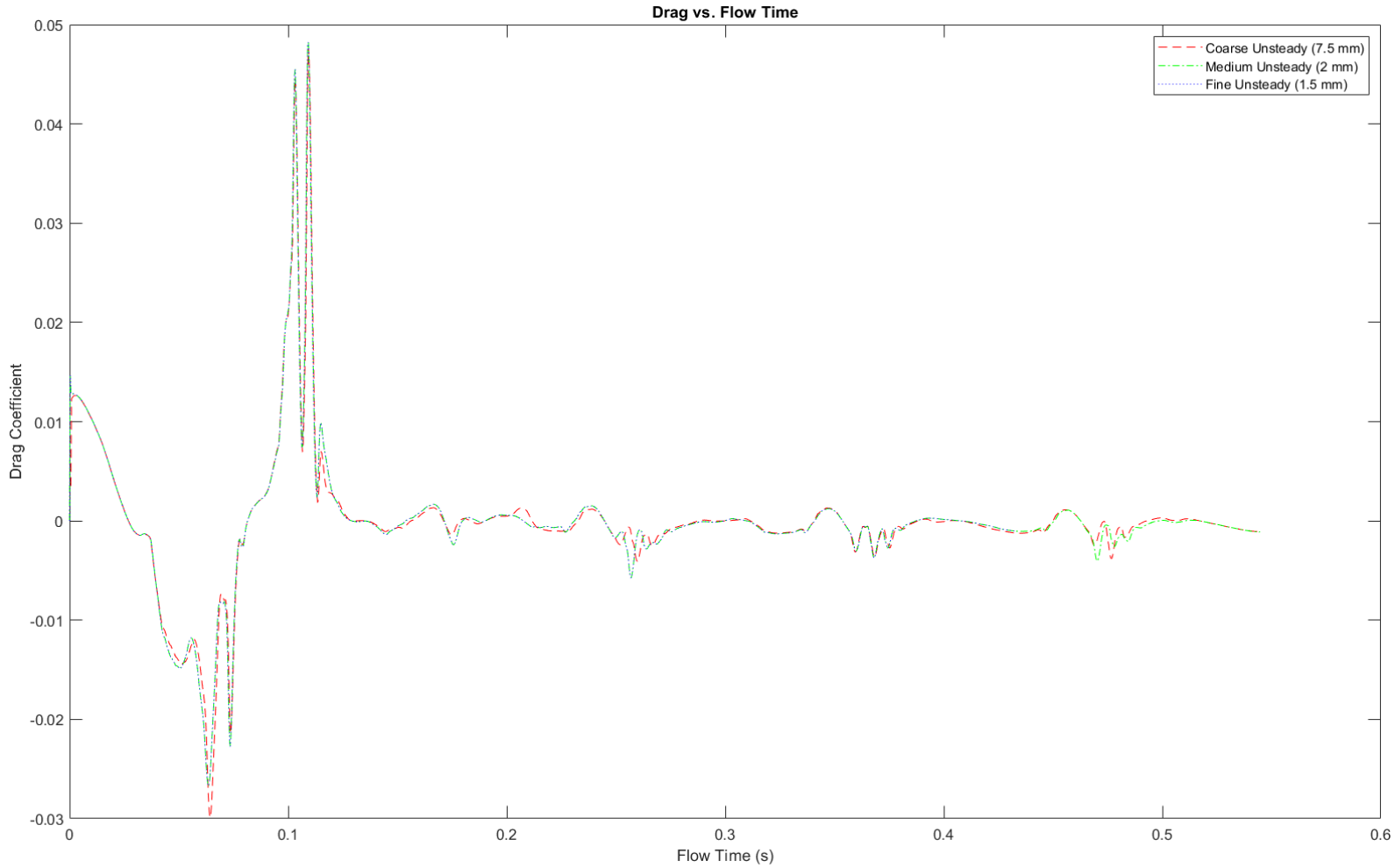


Velocity (at aerofoil) – m/s	29.7
Viscosity – Pa.s	1.81e-5
Chord length – m	0.0858
Density – kg/m^3	1.225
Target y+	1
Number of layers	15
First layer height – m	1.95e-5
Final layer height – m	1.57e-4
Growth rate	1.16

Mesh Validation

- Four meshes of differing resolution were run using the TSST + SBES model. These simulations were not allowed to converge.
  - The meshes were varied by controlling the element size of the body of influence around the aerofoil
- Early flow behaviour was compared to select the mesh to be used for the full simulation run.
- The results were compared to one another, and the second finest mesh (BOI element size = 2mm) was selected.
- This mesh was selected as it was equal in accuracy to the finest mesh(1.5 mm)
- Results of this process can be seen on the next page (drag comparison) and the appendices (full force histories)

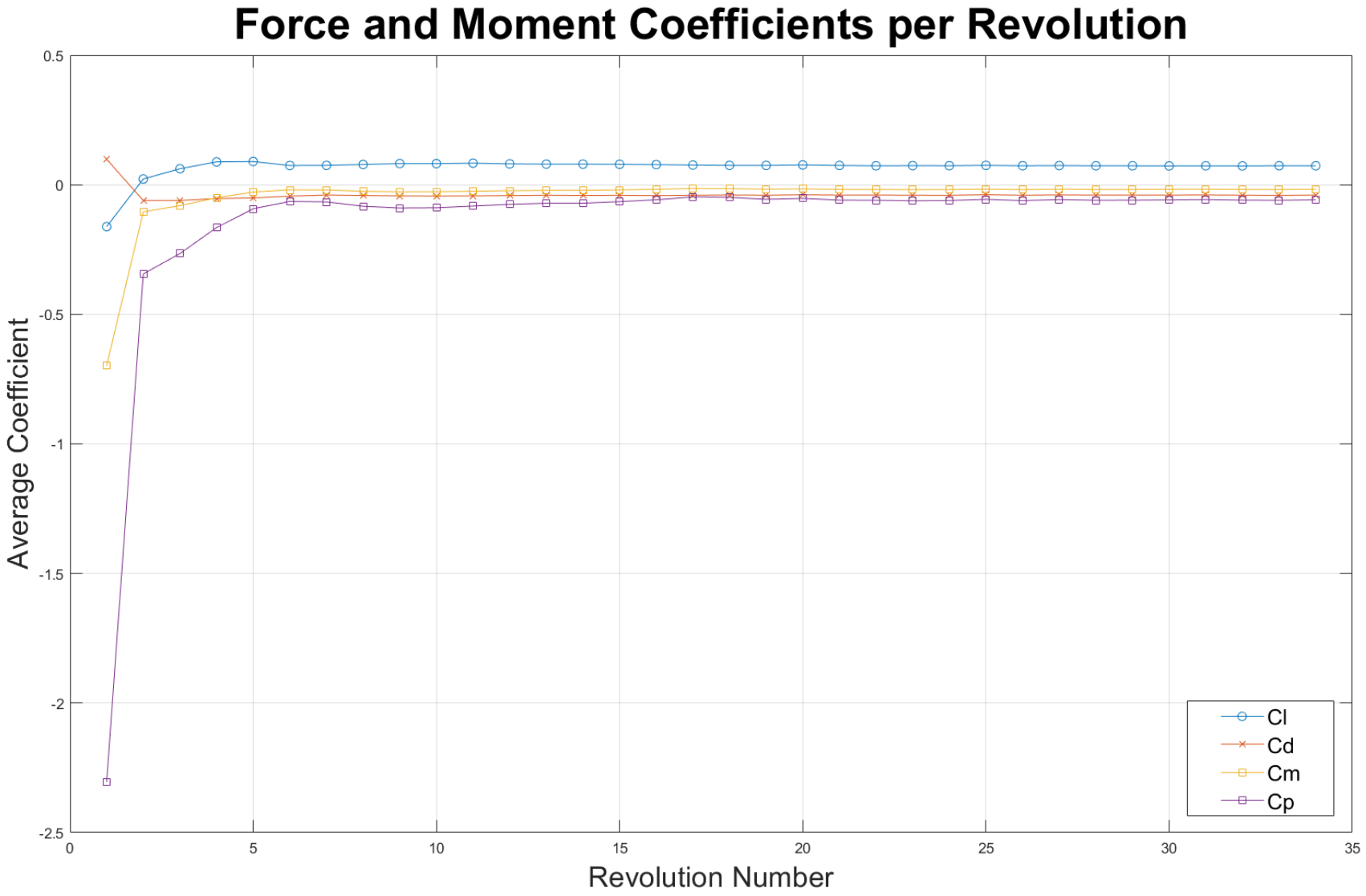
Mesh Comparison



- Cl, Cd, Cm are compared to experimental data
- Cp is compared to reference paper

		Coarse (7.5 mm) % error	Medium (2 mm) % error	Fine (1.5 mm) % error
1	**Power**	0.9273	0.9728	0.9728
2	**Drag**	-0.1199	-0.1258	-0.1258
3	**Lift**	0.0360	0.0347	0.0347
4	**Moment**	-6.1820	-6.4856	-6.4856

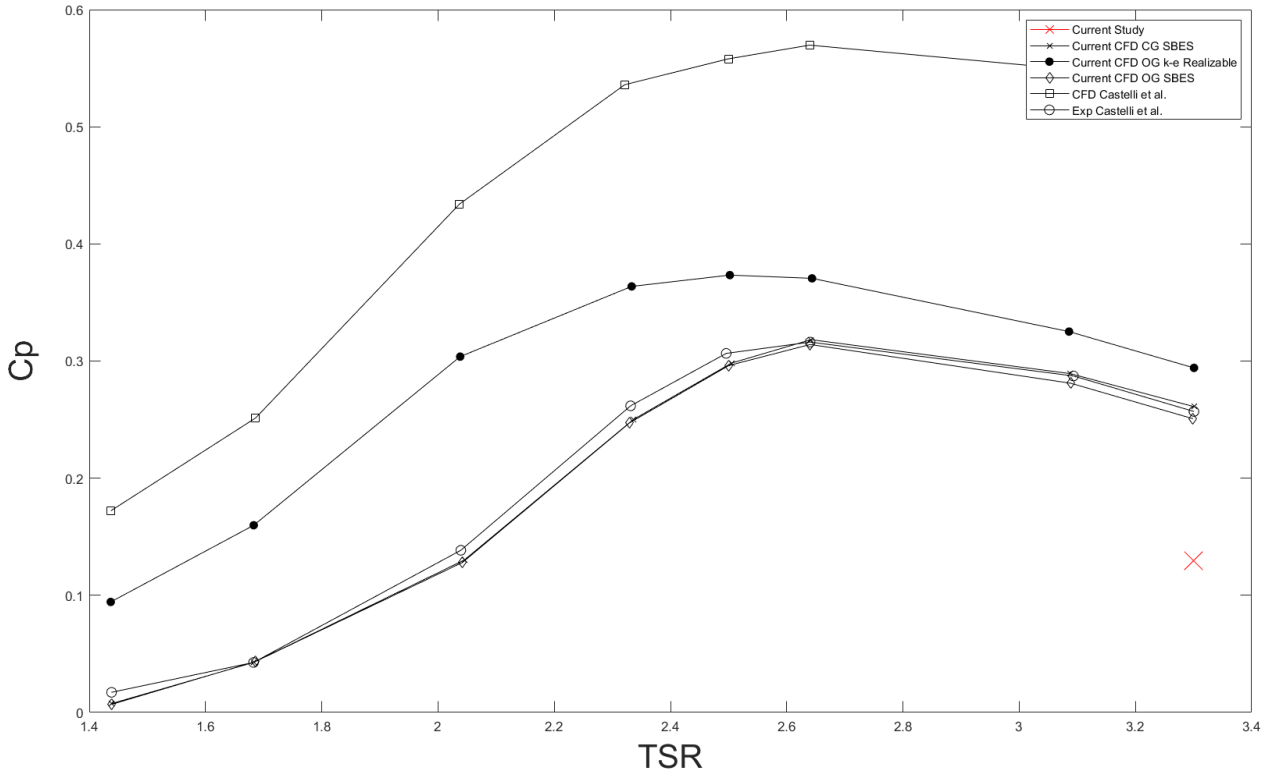
Mesh convergence



Comparison with Primary Paper – Power

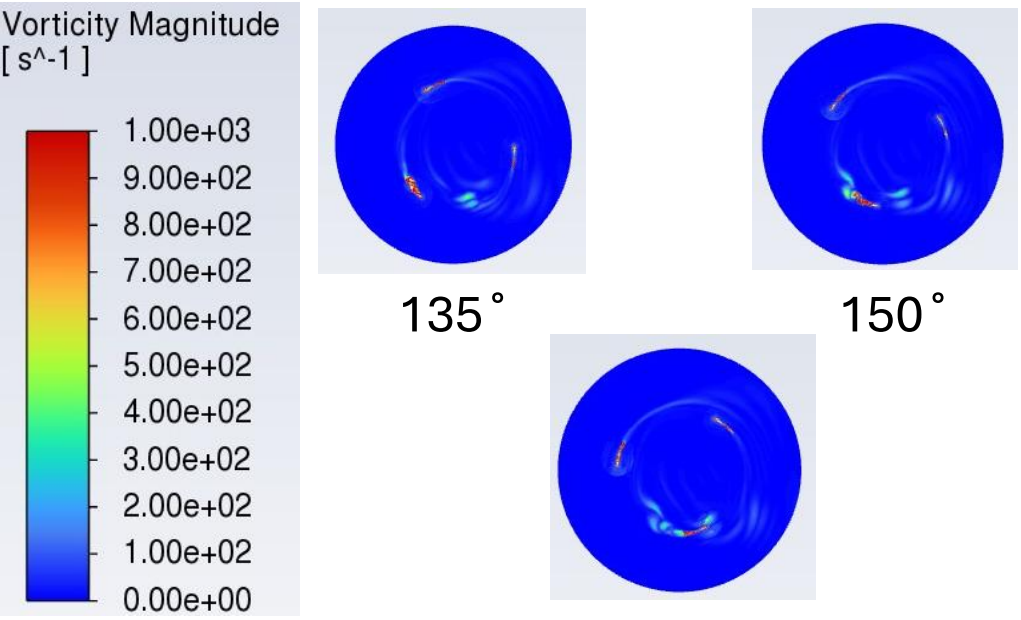
- This study simulated a VAWT at TSR = 3.3. Reference paper simulation explored TSRs between 1.44 and 3.3.
- Syawitri (2020) results are graphical. Approximate position of the power generated by this study's setup is shown below.
- The current study significantly underpredicts Cp (Cp ≈ 0.13 vs Syawitri Cp ≈ 0.27)
  - Lesser computational power used
  - Worse BOI meshing
  - High timestep, combined with less available compute → convergence issues, increased early vorticity dissipation and weaker blade loading

		% Error to Current Study
1	Exp Castelli et al.	49.5900
2	Current CFD CG SBES	50.3900
3	Current CFD OG SBES	48.3400
4	CFD Castelli et al.	75.3900
5	Current CFD OG k-e Realizable	55.9700



Comparison with Primary Paper cont'd – vorticity

- Local Setup features
  - Weaker vortex structures observed
  - Less turbulence in the rotating region
  - Likely cause is worse compute/poorer BOI mesh compared to reference paper

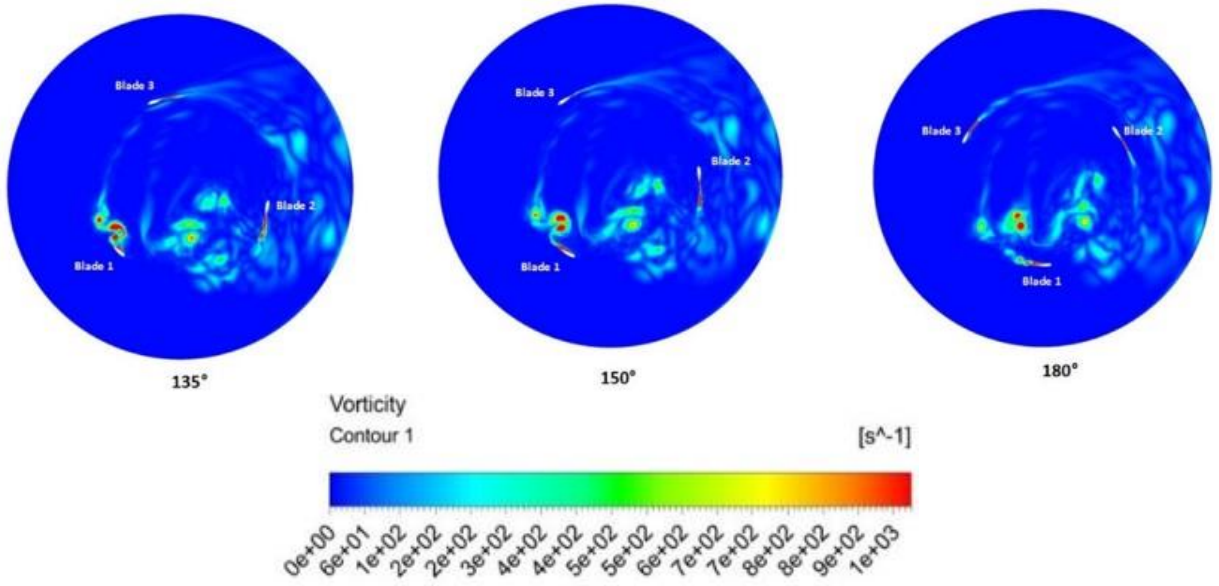


135˚

150˚

180˚

- Reference Paper features
  - Strong vortex structures
  - Turbulence generated by one blade affects flow at tip for next blade
  - Likely reason: higher fidelity BOI mesh able to resolve fine vortex shedding. Better compute used to perform simulation



Discussion of Aerodynamic Results

- Cp underprediction of likely stems from insufficient mesh resolution in the BOI, which reduced vortex strength and disrupted wake development.
- While the all force and power coefficients stabilised over multiple revolutions, the pressure field lacked the intensity and gradient sharpness expected in the shedding zones.
- This suggests the presence of numerical damping due to both a poor spatial resolution and a relatively large timestep (Δt = 3e-4 s).
- These factors suppress the amplitude of pressure oscillations, which in turn lowers aerodynamic forces and Cp output.

Time-step Considerations and Implications

- Syawitri et. al. (2020) uses a 1 degree timestep. $\Delta t \approx 3 \times 10^{-4}$ s
- This timestep is relatively high and will lead to larger courant numbers as well as relatively less accurate results.
- Case courant cell number = ~ 10 is above the acceptable range for TSST + SBES model. Ideally, courant cell number < 1 (Ansys Fluent Theory Guide, 2025).
- Reason for high courant number → relatively high time-step. Ideally, time-step <0.5 ° ≈ 10^{-5} s. Thus decreasing solver instability and allowing for finer data capture.

$$\Delta t = \frac{\theta}{\omega} = \frac{\pi/_{180}}{\omega}$$

In acoustic simulation, timesteps dictate the maximum resolvable frequency.
The Nyquist criterion calculates this frequency.

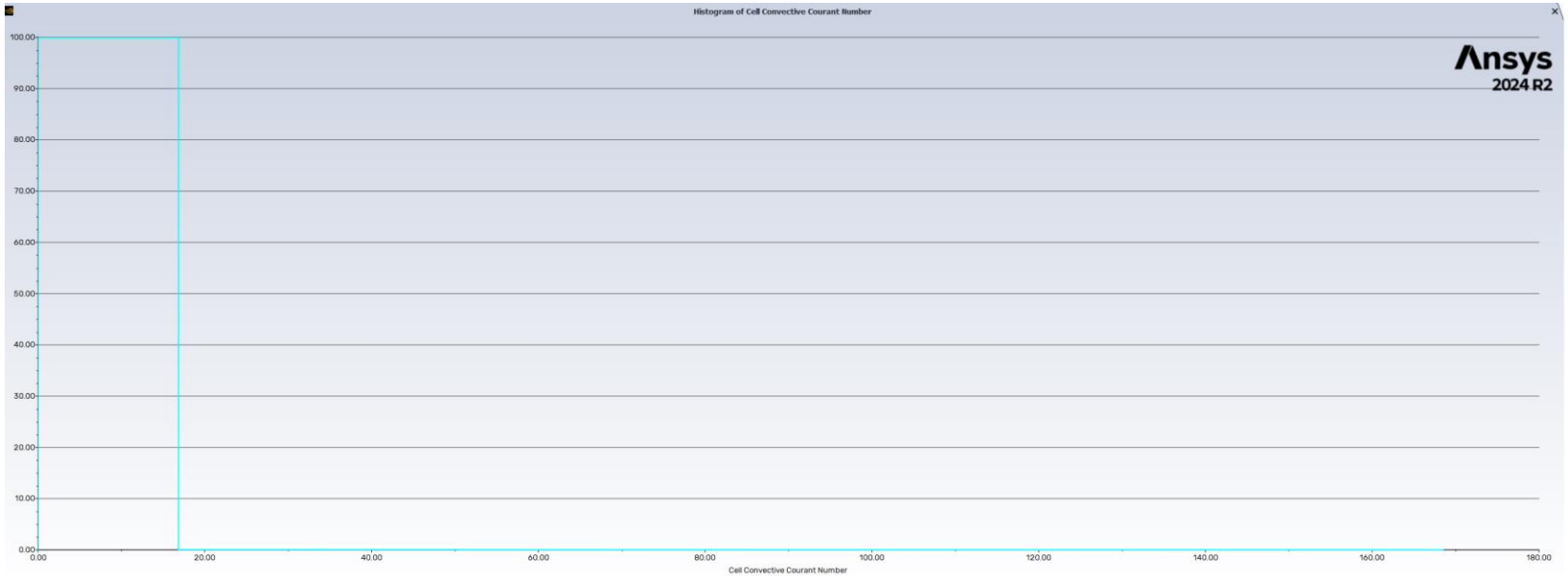
Nyquist frequency:

$$f_{max} = \frac{1}{2\Delta t}$$

This study:

$$f_{max} = \frac{1}{2 \times 3e^{-4}}$$

$$\approx 1667Hz$$



This is below the audible range for humans(20Hz – 20kHz) meaning:

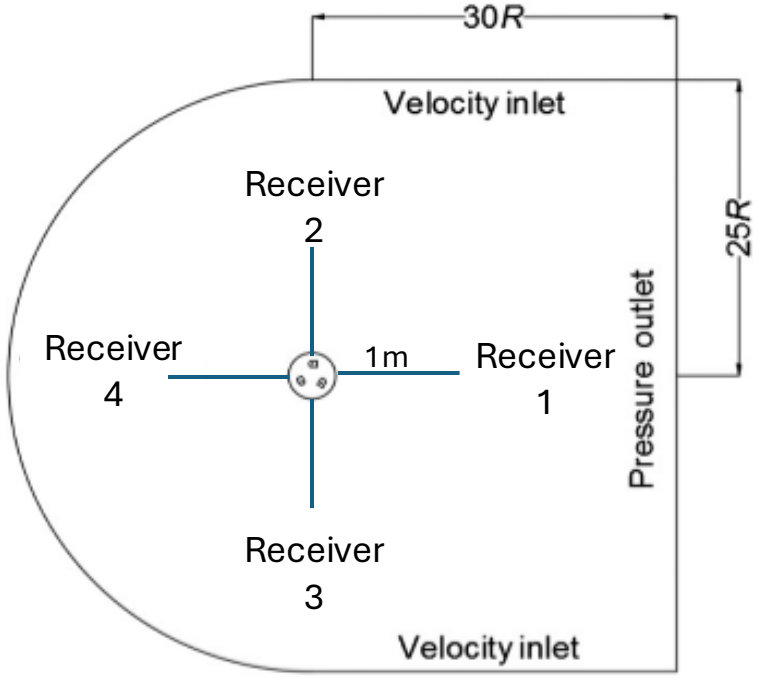
- Unresolved higher-order harmonics
- Dampened broadband noise

Acoustic Setup

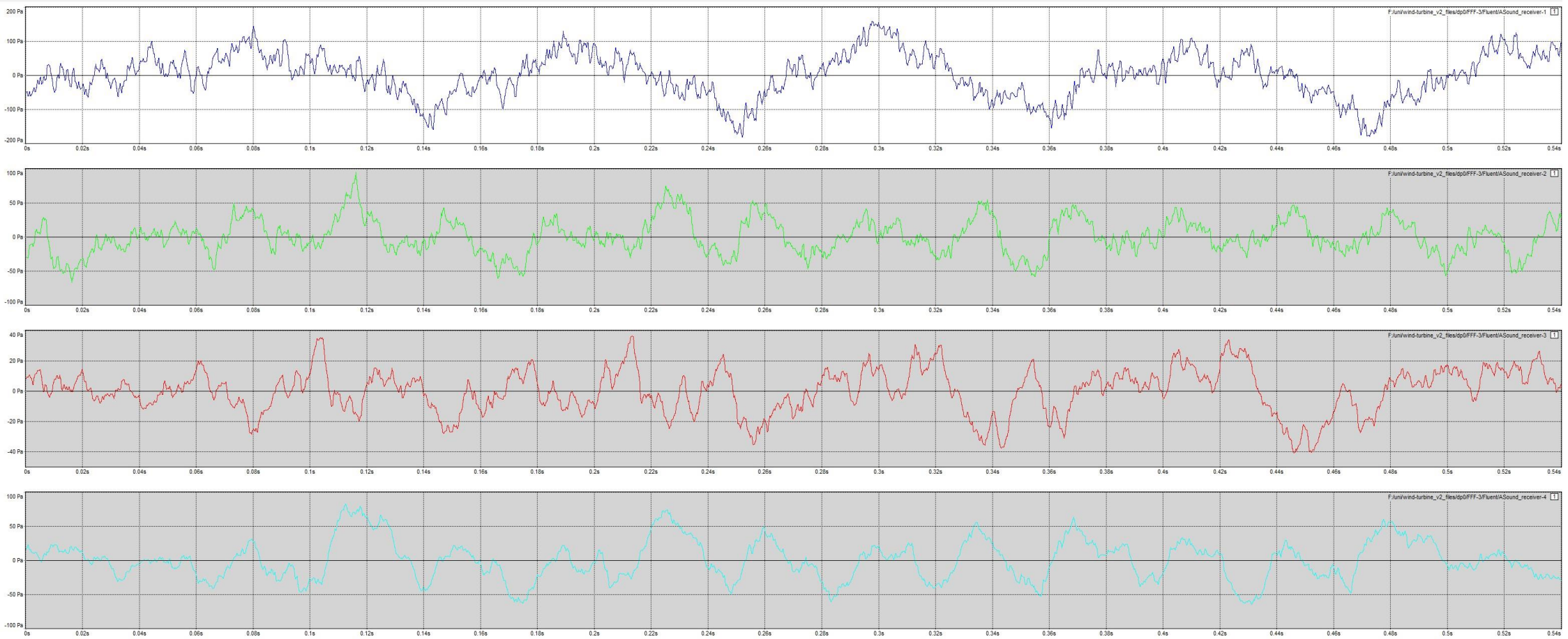
- The FW-H acoustic analogy was used to predict the nose generated by the simulated setup. This analogy is a modification of Lighthill's wave equation as can be seen below (ANSYS Fluent Theory Guide, 2025):
- FW-H is well-suited to low mach flows

$$\frac{1}{a_0^2}\frac{\partial^2 p'}{\partial t^2} - \nabla^2 p' = \frac{\partial^2}{\partial x_i \partial x_j}\{T_{ij}H(f)\} - \frac{\partial}{\partial x_i}\{[P_{ij}n_j + \rho u_i(u_n - v_n)]\,\delta(f)\} + \frac{\partial}{\partial t}\{[\rho_0 v_n + \rho(u_n - v_n)]\,\delta(f)\}$$

Source correlation length (m)	0.0858
Source Zone	Rotating domain
Freestream velocity (m/s)	9
Farfield density (kg/m^3)	1.225
Far-field sound speed (m/s)	340
Reference acoustic pressure (Pa)	2e^{-5}



Pressure vs Time History



Receiver 1

Receiver 2

Receiver 3

Receiver 4

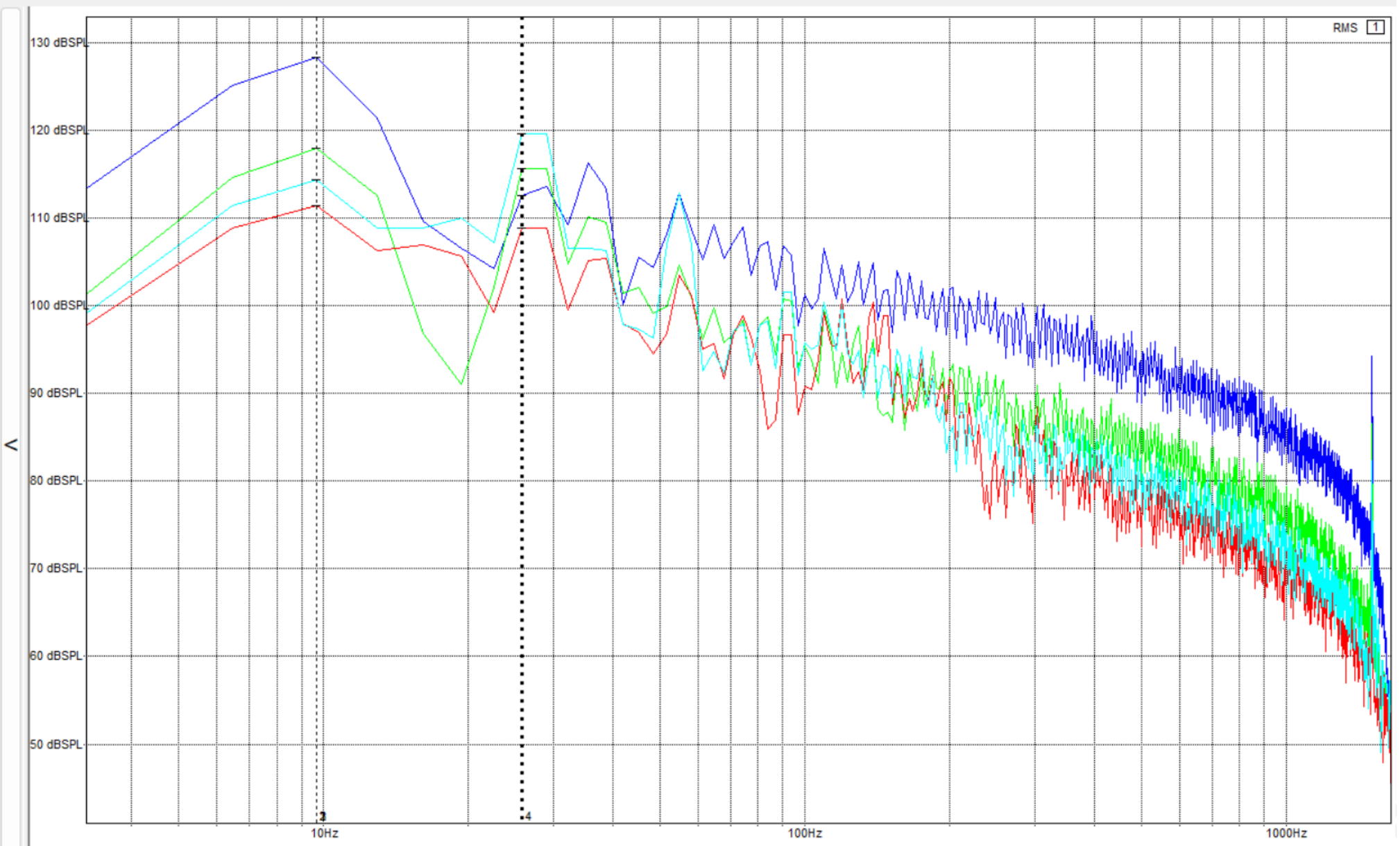
Purpose: Validate that data generated is valid and usable for further analysis

Peak pressure seen at receiver 1 ≈ 155Pa

Acoustic Results – SPL vs frequency

Information | Cursors

	N.	Position (Hz)	1	1
▼	1	9.683	128.3340	118.0128
▼	2	9.683	128.3340	118.0128
▼	3	9.683	128.3340	118.0128
▼	4	25.820	112.5663	115.6787



Acoustic Analysis

- Theoretical blade passing frequency calculated using: BPF = (blade count*RPM)/60
- Upstream receiver (4) sees cleaner BPF tones due to tonal noise propagating downstream
- Receiver 1 – downstream is placed in the wake region
  - Low frequency noise dominates
  - BPF tones unclear due to wake-induced broadband tones(Moreau & Roger, 2007)
- Downstream receivers capture low frequency tones, due to wake turbulence and unsteady blade loading according to Gros et. al (2020)
- Discrepancies between theoretical and observed BPF likely due to mesh-induced smoothing

Receiver name	x-coordinate location (m)	Calculated BPF (Hz)	Rotational frequency (Hz)	SPL (dB)	BPF % error
1	1	27.54	9.68	128.33	-5.49
2	1	27.54	9.68	128.33	-5.49
3	-1	27.54	9.68	128.33	-5.49
4	-1	27.54	25.82	112.56	6.23

Conclusion

- Due to computational constraints, the simulation used a timestep of Δt = 3×10^{-4} s, which restricts the upper frequency limit of resolved acoustic data to approximately 1.67 kHz (Nyquist frequency). As a result, the simulation under samples the full human-audible range (20 Hz – 20 kHz), missing high-frequency components that are important for urban annoyance prediction and sensor interference (e.g. autonomous vehicle microphones).
- This limitation leads to several issues:
  - Resolution loss at frequencies above ~1.5 kHz
  - Under-representation of high-frequency tonal peaks from laminar-turbulent transitions
  - A bias towards low-frequency, wake-driven broadband noise, especially at downstream receivers

Nyquist frequency:

$$f_{max} = \frac{1}{2\Delta t}$$

This study:

$$f_{max} = \frac{1}{2 \times 3e^{-4}} \approx 1667Hz$$

Future Work

- This study only investigated the noise generated by a VAWT. Future investigations should expand on this foundation to capture higher frequencies to avoid the disruption of urban animals (pets, strays etc.) and sensitive technology (e.g. sensor arrays on self driving vehicles)
- 3D studies using more refined meshes should be conducted to understand the complex VAWT flow (blade-vortex interactions, dynamic stall) and fully predict noise.
- The current study under samples the audible range for humans as the timestep used is too high ($3e^{-4}$s). Lower end requires timestep = $2.5e^{-4}$s. Future studies should aim to capture the full range of frequencies audible to the human ear
- Future studies should include Q-criterion or λ_2 visualisation to better resolve vortex-acoustic correlation, especially for identifying trailing-edge shedding or dynamic stall events that contribute to tonal noise.

References

ANSYS (2009) *ANSYS FLUENT 12.0 Theory Guide - 4.11.2 Filtered Navier-Stokes Equations ANSYS FLUENT 12.0 Theory Guide*. 29 January 2009 [online]. Available from: https://www.afs.enea.it/project/neptunius/docs/fluent/html/th/node94.htm [Accessed 13 June 2025].

ANSYS Inc. (2025) - *Ansys Help Ansys.com*. 2025 [online]. Available from: https://ansyshelp.ansys.com/public/account/secured?returnurl=/Views/Secured/corp/v242/en/flu_th/flu_th_turb_sbes_intro.html [Accessed 1 June 2025].

ANSYS Inc. (2021) *Ansys CFX-Solver Theory Guide* [online]. Available from: https://dl.cfdexperts.net/cfd_resources/Ansys_Documentation/CFX/Ansys_CFX-Solver_Theory_Guide.pdf [Accessed 1 June 2025].

Castelli, M.R., Ardizzon, G., Battisti, L., Benini, E. and Pavesi, G. (2010), "Modeling strategy and numerical validation for a Darrieus Vertical Axis Micro-Wind Turbine", Fluid Flow, Heat Transfer and Thermal Systems, Parts A and B Proceeding of ASME 2010 International Mechanical Engineering Congress and Exposition in Vancouver, British Columbia, Canada, 2010, ASME, Vancouver, Vol. 7, pp. 409-418.

'Fluid Mechanics 101' (no date) *www.fluidmechanics101.com* [online]. Available from: https://www.fluidmechanics101.com/pages/tools.html [Accessed 14 November 2024].

Ma, L., Wang, X., Zhu, J. and Kang, S. (2019) Dynamic Stall of a Vertical-Axis Wind Turbine and Its Control Using Plasma Actuation. *Energies* [online]. 12 (19), p. 3738. Available from: https://www.mdpi.com/1996-1073/12/19/3738 [Accessed 25 June 2025].

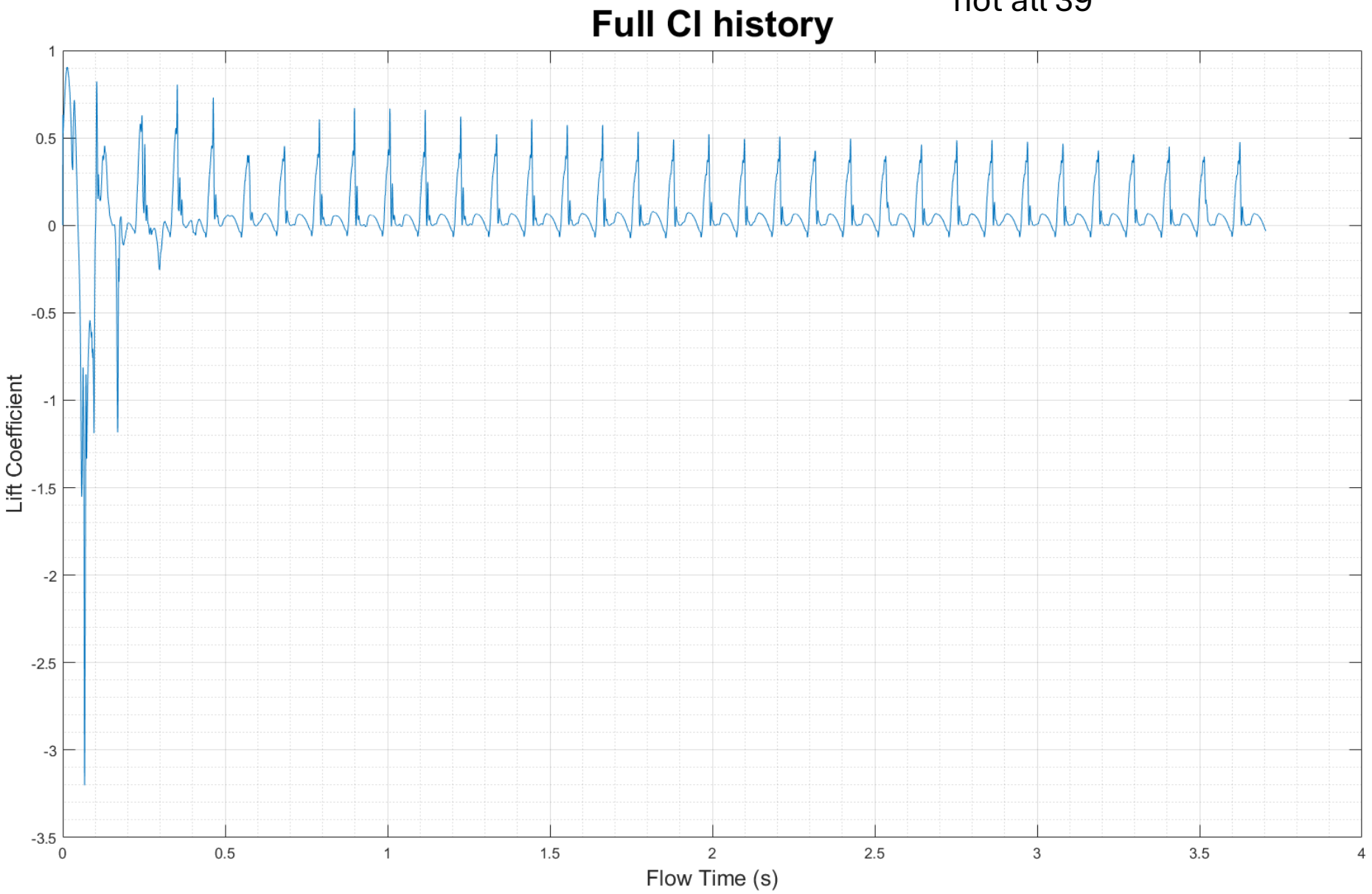
Syawitri, T.P., Yao, Y., Yao, J. and Chandra, B. (2020) Assessment of stress-blended eddy simulation model for accurate performance prediction of vertical axis wind turbine. *International Journal of Numerical Methods for Heat & Fluid Flow* [online]. 31 (2), pp. 655–673. [Accessed 13 November 2024].

ANSYS RUN(only the final one, the validation files are corrupt and cannot be opened/moved to onedrive): https://uweacuk-my.sharepoint.com/:f:/g/personal/linus2_adzanku_live_uwe_ac_uk/EhQoAUfUCnxKuw4DN2doLq4Biz69UXJTIbrbD_DlNzVwsQ?e=UJNA2k

Appendices

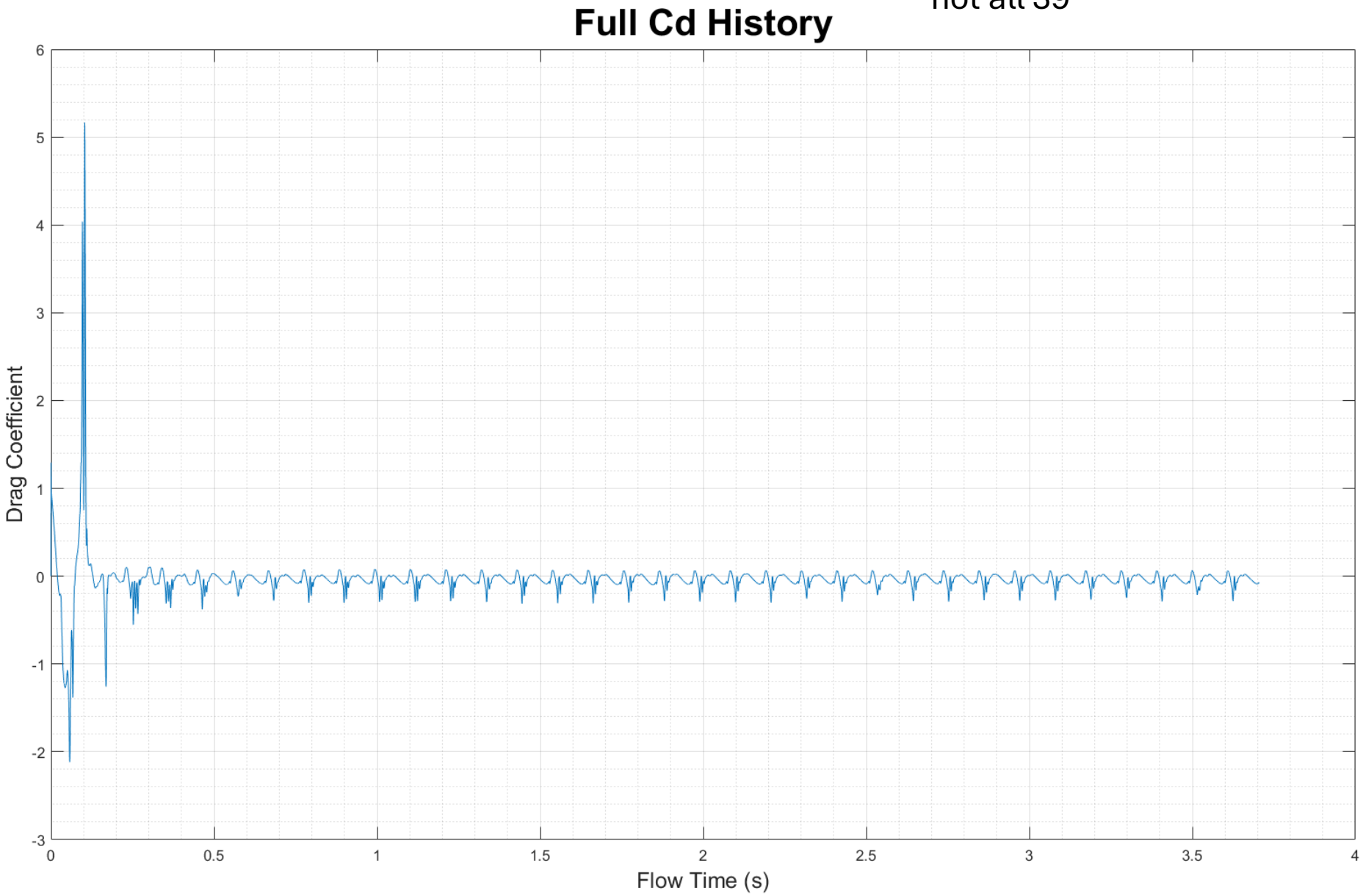
Full Force History - Cl

* Data used is for 34 rotor revolutions, not all 39



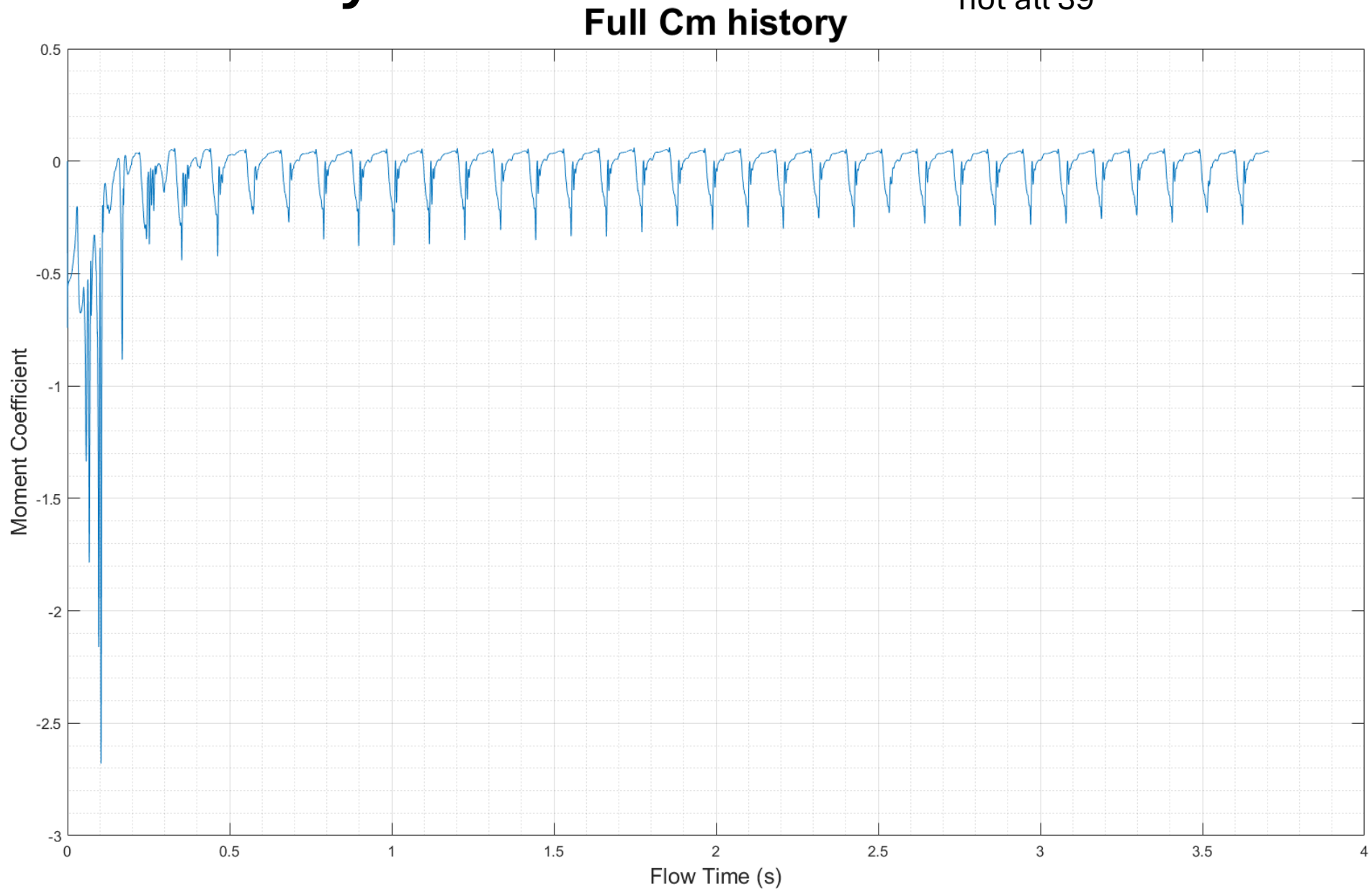
Full Force History - Cd

* Data used is for 34 rotor revolutions, not all 39



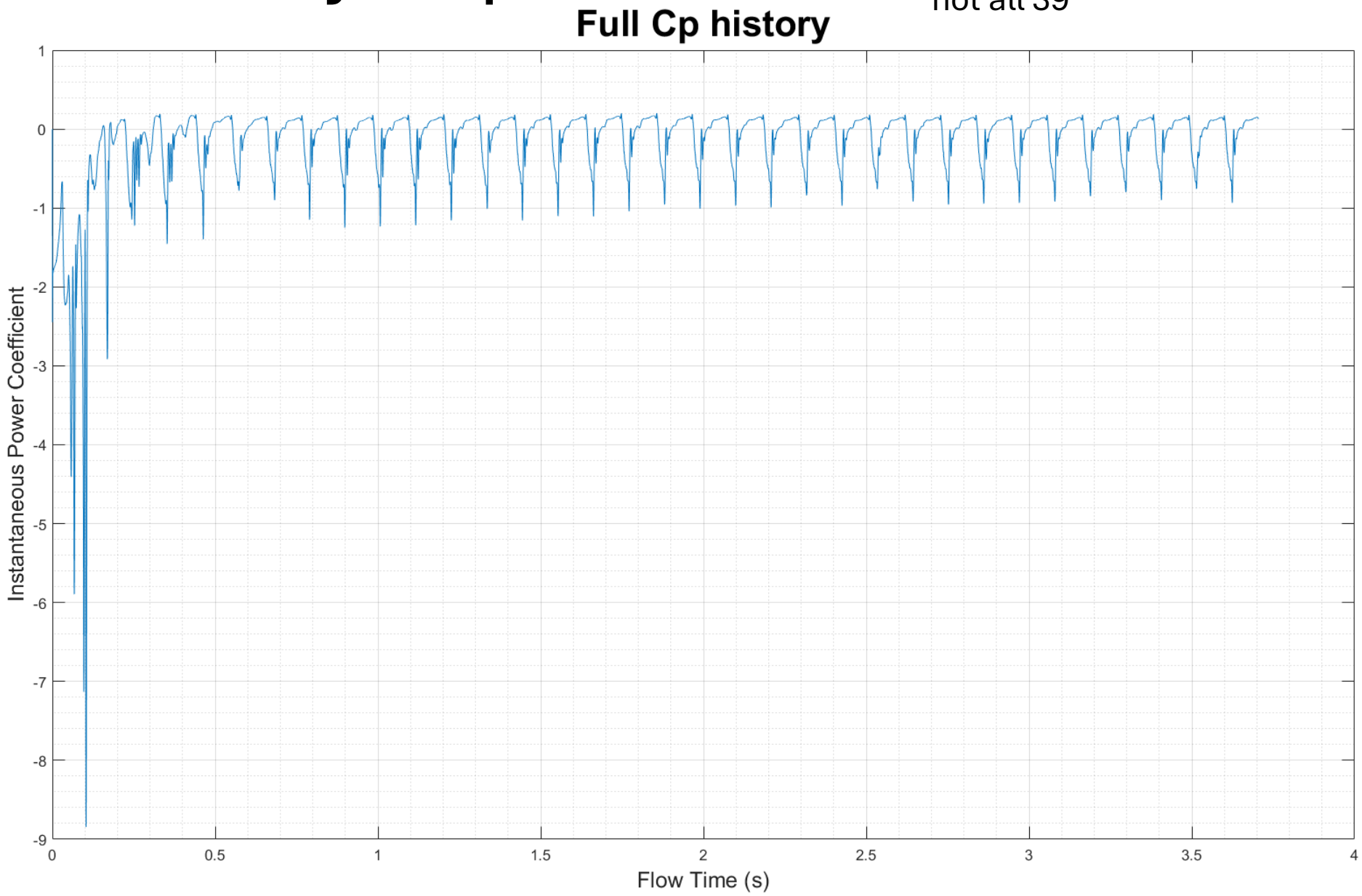
Full Force History - Cm

* Data used is for 34 rotor revolutions, not all 39

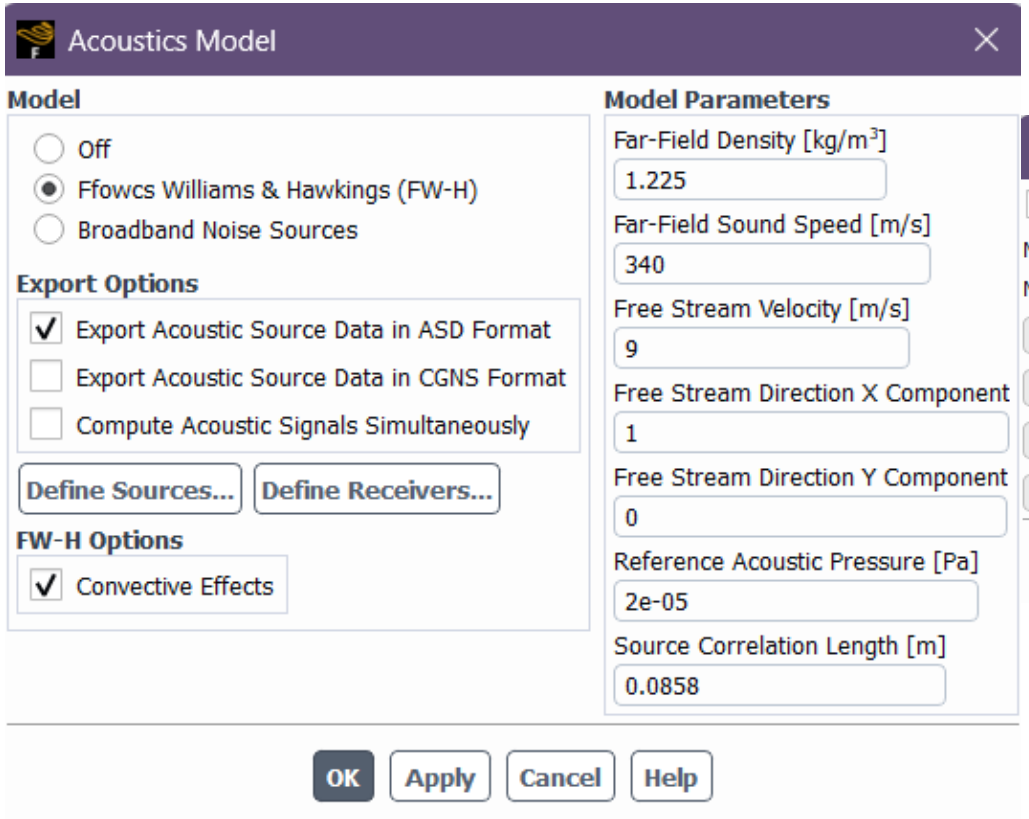


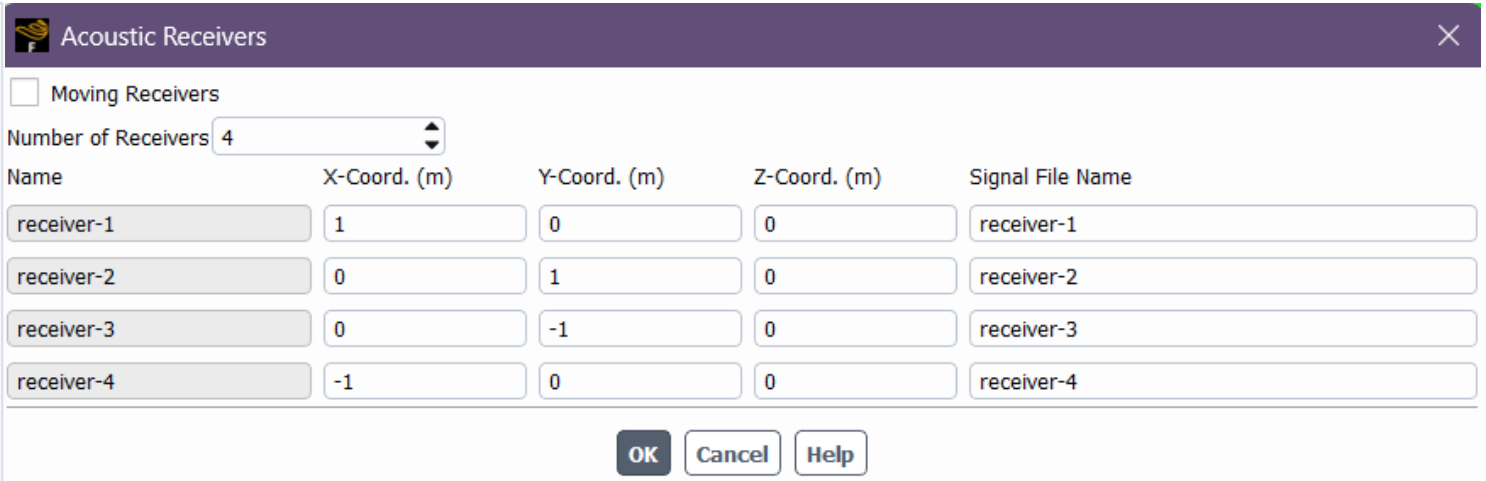
Full Force History - Cp

* Data used is for 34 rotor revolutions, not all 39

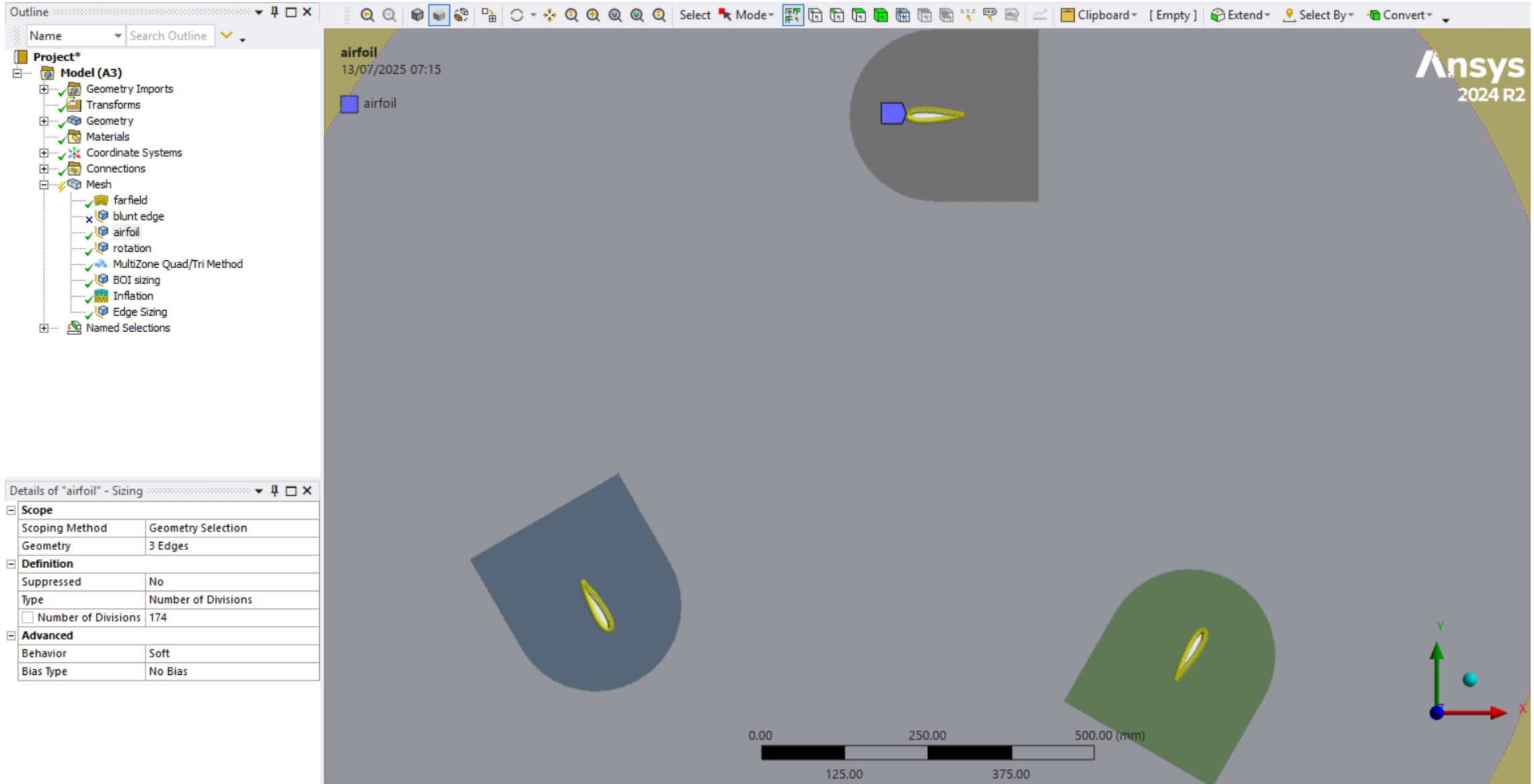


Acoustic Setup Parameters





Mesh Structure Setup Parameters



Outline

Name | Search Outline

- Project
  - Model (A3)
    - Geometry Imports
    - Transforms
    - Geometry
    - Materials
    - Coordinate Systems
    - Connections
    - Mesh
      - farfield
      - blunt edge
      - airfoil
      - rotation
      - MultiZone Quad/Tri Method
      - BOI sizing
      - Inflation
      - Edge Sizing
    - Named Selections

Details of "farfield" - Mapped Face Meshing

Scope	
Scoping Method	Geometry Selection
Geometry	6 Faces
Definition	
Suppressed	No
Mapped Mesh	Yes
Method	Quadrilaterals
Constrain Boundary	No
Advanced	
Specified Sides	No Selection
Specified Corners	No Selection
Specified Ends	No Selection
MultiZone Semi-Structured	No

Project
Model (A3)
Geometry Imports
Transforms
Geometry
Materials
Coordinate Systems
Connections
Mesh
farfield
blunt edge
airfoil
rotation
MultiZone Quad/Tri Method
BOI sizing
Inflation
Edge Sizing
Named Selections

Details of "Mesh"

Display	
Display Style	Use Geometry Setting
Defaults	
Physics Preference	CFD
Solver Preference	Fluent
Element Size	50.0 mm
Export Format	Standard
Export Preview Surface Mesh	No
Sizing	
Quality	
Inflation	
Batch Connections	
Advanced	
Statistics	

Outline

Name | Search Outline

- Project*
  - Model (A3)
    - Geometry Imports
    - Transforms
    - Geometry
    - Materials
    - Coordinate Systems
    - Connections
    - Mesh
      - farfield
      - blunt edge
      - airfoil
      - rotation
      - MultiZone Quad/Tri Method
      - BOI sizing
      - Inflation
      - Edge Sizing
    - Named Selections

Details of "Edge Sizing" - Sizing

Scope	
Scoping Method	Geometry Selection
Geometry	4 Edges
Definition	
Suppressed	No
Type	Element Size
Element Size	50.0 mm
Advanced	
Behavior	Soft
Bias Type	----- --- - -
Bias Option	Bias Factor
Bias Factor	15.0
Reverse Bias	No Selection

Select | Mode | Clipboard | [Empty] | Extend | Select By | Convert

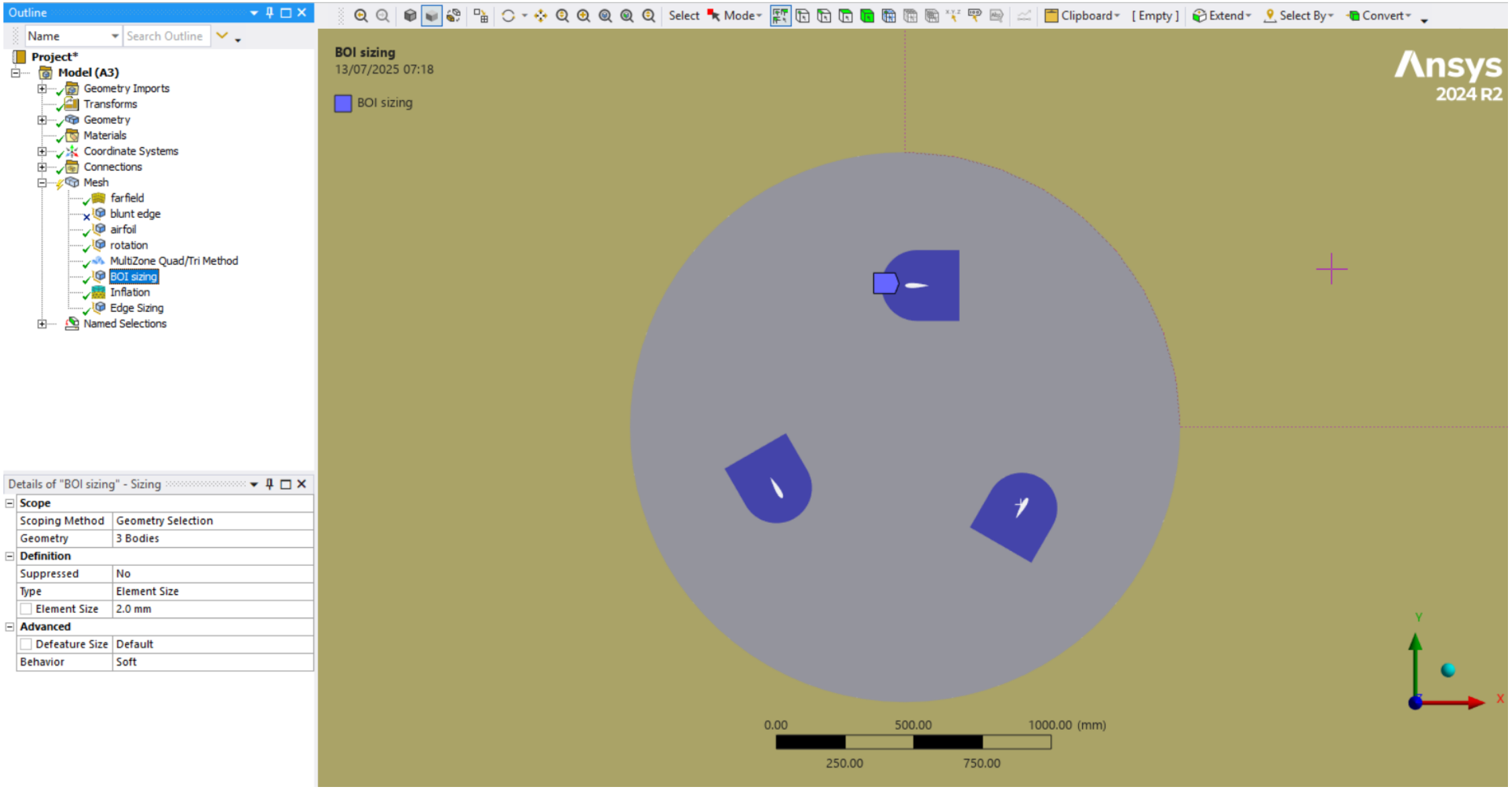
Edge Sizing
13/07/2025 07:19

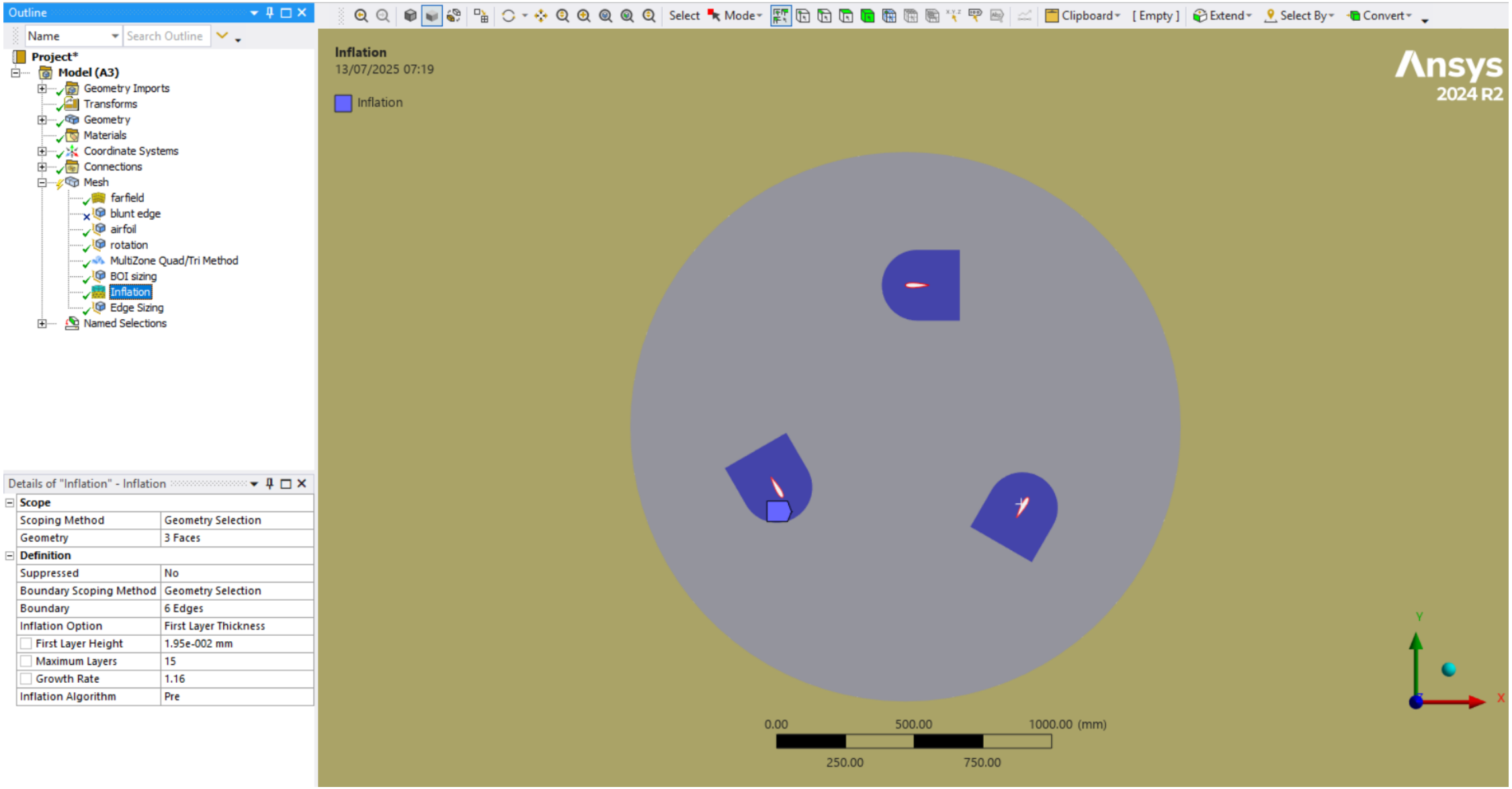
Edge Sizing

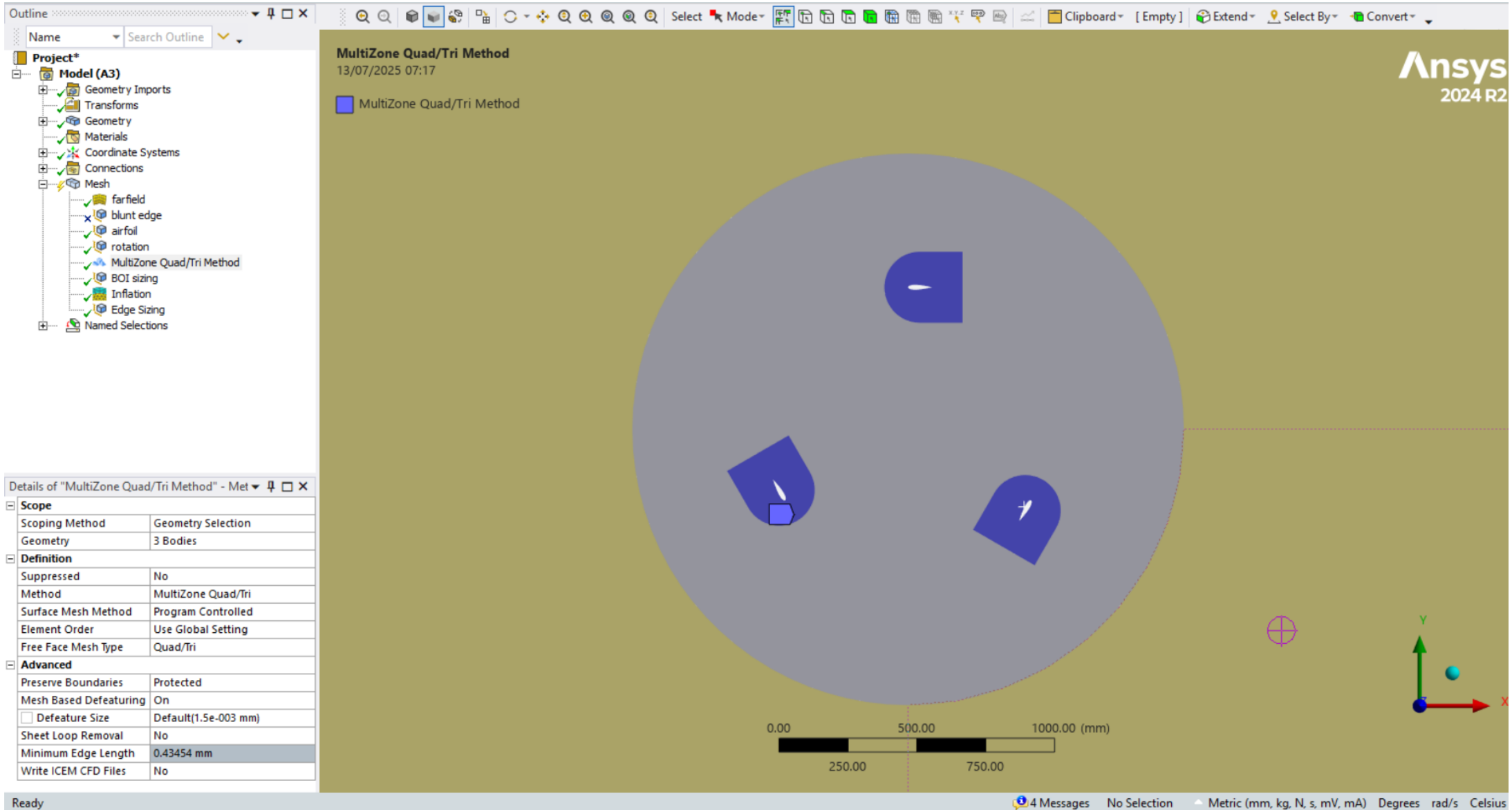
Ansys
2024 R2

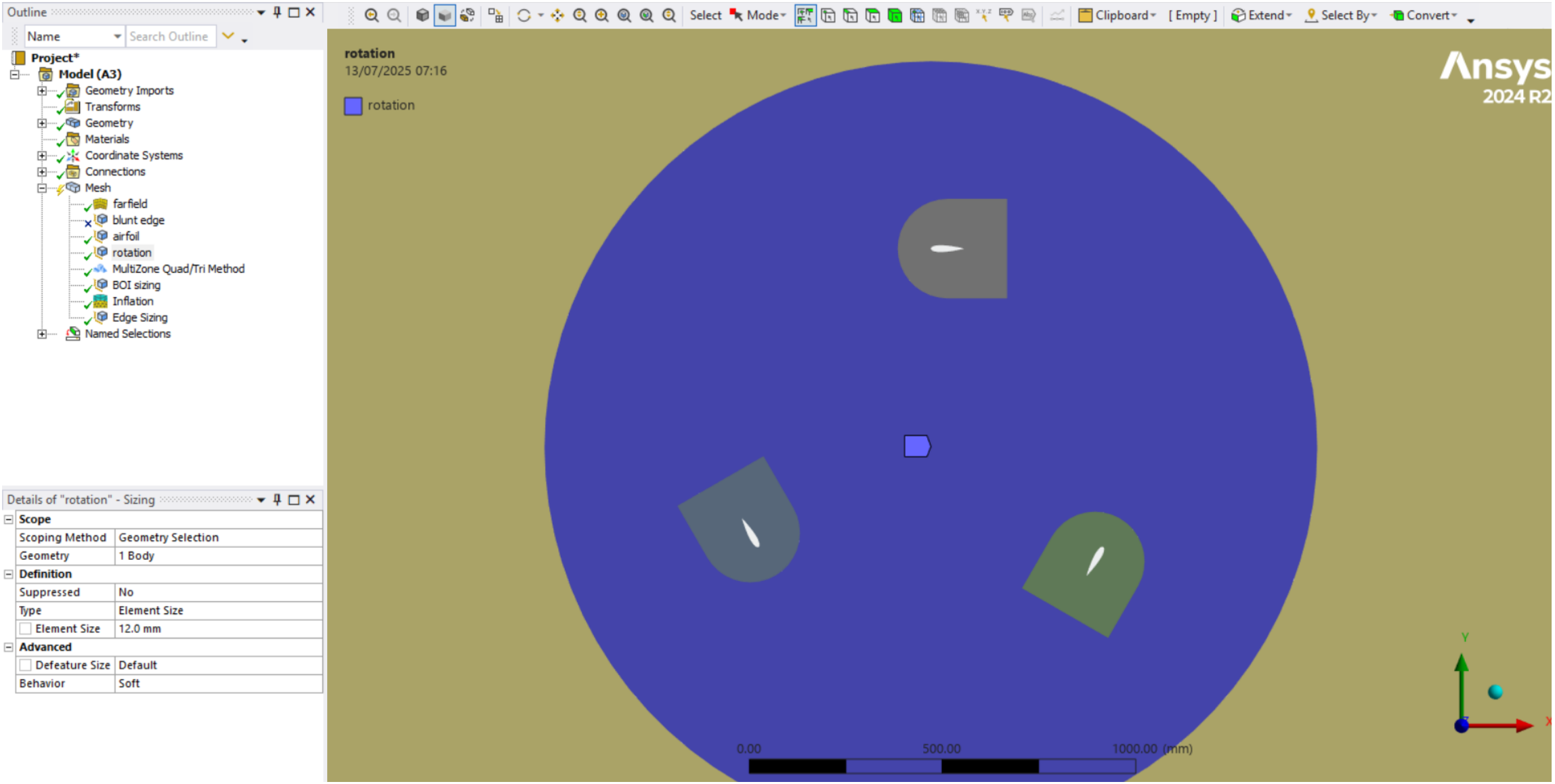
0 5e+03 1e+04 (mm)
2.5e+03 7.5e+03

Y
X


Outline
Name
Search Outline
Project*
Model (A3)
Geometry Imports
Transforms
Geometry
Materials
Coordinate Systems
Connections
Mesh
farfield
blunt edge
airfoil
rotation
MultiZone Quad/Tri Method
BOI sizing
Inflation
Edge Sizing
Named Selections
Details of "BOI sizing" - Sizing
Scope
Scoping Method
Geometry Selection
Geometry
3 Bodies
Definition
Suppressed
No
Type
Element Size
Element Size
2.0 mm
Advanced
Defeature Size
Default
Behavior
Soft
Select
Mode
Clipboard
[Empty]
Extend
Select By
Convert
BOI sizing
13/07/2025 07:18
BOI sizing
Ansys
2024 R2
0.00
500.00
1000.00 (mm)
250.00
750.00
Y
X


Outline
Name
Search Outline
Project*
Model (A3)
Geometry Imports
Transforms
Geometry
Materials
Coordinate Systems
Connections
Mesh
farfield
blunt edge
airfoil
rotation
MultiZone Quad/Tri Method
BOI sizing
Inflation
Edge Sizing
Named Selections
Select
Mode
Clipboard
[Empty]
Extend
Select By
Convert
Inflation
13/07/2025 07:19
Inflation
Ansys
2024 R2
Details of "Inflation" - Inflation
Scope
Scoping Method
Geometry Selection
Geometry
3 Faces
Definition
Suppressed
No
Boundary Scoping Method
Geometry Selection
Boundary
6 Edges
Inflation Option
First Layer Thickness
First Layer Height
1.95e-002 mm
Maximum Layers
15
Growth Rate
1.16
Inflation Algorithm
Pre
0.00
500.00
1000.00 (mm)
250.00
750.00
Y
X


Outline
Name
Search Outline
Project*
Model (A3)
Geometry Imports
Transforms
Geometry
Materials
Coordinate Systems
Connections
Mesh
farfield
blunt edge
airfoil
rotation
MultiZone Quad/Tri Method
BOI sizing
Inflation
Edge Sizing
Named Selections
Details of "MultiZone Quad/Tri Method" - Met
Scope
Scoping Method | Geometry Selection
Geometry | 3 Bodies
Definition
Suppressed | No
Method | MultiZone Quad/Tri
Surface Mesh Method | Program Controlled
Element Order | Use Global Setting
Free Face Mesh Type | Quad/Tri
Advanced
Preserve Boundaries | Protected
Mesh Based Defeaturing | On
Defeature Size | Default(1.5e-003 mm)
Sheet Loop Removal | No
Minimum Edge Length | 0.43454 mm
Write ICEM CFD Files | No
Select
Mode
Clipboard
[Empty]
Extend
Select By
Convert
MultiZone Quad/Tri Method
13/07/2025 07:17
MultiZone Quad/Tri Method
Ansys
2024 R2
0.00
500.00
1000.00 (mm)
250.00
750.00
Y
X
Ready
4 Messages
No Selection
Metric (mm, kg, N, s, mV, mA)
Degrees
rad/s
Celsius


Outline
Name
Search Outline
Project*
Model (A3)
Geometry Imports
Transforms
Geometry
Materials
Coordinate Systems
Connections
Mesh
farfield
blunt edge
airfoil
rotation
MultiZone Quad/Tri Method
BOI sizing
Inflation
Edge Sizing
Named Selections
Details of "rotation" - Sizing
Scope
Scoping Method
Geometry Selection
Geometry
1 Body
Definition
Suppressed
No
Type
Element Size
Element Size
12.0 mm
Advanced
Defeature Size
Default
Behavior
Soft
Select
Mode
Clipboard
[Empty]
Extend
Select By
Convert
rotation
13/07/2025 07:16
rotation
Ansys
2024 R2
0.00
500.00
1000.00 (mm)
Y
X